6 結言

本研究は、放射性薬剤への調製の工程を作成し、従来の装置に追加することによって、放射性薬剤 ^{64}Cu-ATSM の完全自動化を行った。それにより被曝量を軽減し安全性を高めることができ、高放射能ハンドリングに適した研究用ロボットの利用例の 1 つを示すことができた。またプログラム作成メソッドの簡易化によって、開発者だけではなく、実際に装置を使うユーザー側においても、新たな動作工程の作成が可能になり、汎用性も大きく向上できたと考えられる。今後の展望としては、^{64}Cu-ATSM の合成実験を繰り返し、実験条件を確率する予定である。さらに、この装置の汎用性を利用して、医療現場においてガン診断用の薬剤として広く使われている放射性薬剤 ^{18}F-fluorodeoxy glucose(FDG) など、^{18}F を標識する薬剤の合成を行う予定である。

参考文献

1) Tanaka T, Furukawa T, Fujieda S, Kasamatsu S, Yonekura Y, Fujibayashi Y, Double-tracer autoradiography with Cu-ATSM/FDG and immunohistochemical interpretation in four different mouse implanted tumor models, Nucl Med Biol, Vol.33, pp.743-50, 2006

2) McCarthy DW, Shefer RE, Klinkowstein RE, Bass LA, Margeneau WH, Cutler CS, Anderson CJ, Welch MJ, Efficient production of high specific activity ^{64}Cu using a biomedical cyclotron, Nucl Med Biol, Vol.24, pp.35-43, 1997

3) Obata A, Kasamatsu S, McCarthy DW, Welch MJ, Saji H, Yonekura Y, Fujibayasi Y, Production of therapeutic quantities of ^{64}Cu using a 12 MeV cyclotron, Nucl Med Biol, Vol.5, pp.535-539, 2003

4) 楠岡英夫、西村恒彦、藤林靖久、田口政俊、天野昌治、核医学イメージング、コロナ社、2001

5) RCB-3 電子マニュアル

謝辞

本論文を完成するにあたり、懇切丁寧に御指導をいただきました浅井竜哉准教授に心から感謝いたします。また福井大学高エネルギー医学研究センターの藤林靖久教授ならびに森哲也助教には、研究計画から実験指導並びに論文指導まで、懇切丁寧にご指導いただきましたことを深く感謝いたします。また ^{64}Cu 精製装置について懇切丁寧に指導していただいた、卒業された平山大祐氏、その他同センターの方々には心より深く感謝いたします。装置の製作に協力していただいた近藤巧社、京藤樹脂技研社の皆様に深くお礼申し上げます。また友人として共に切磋琢磨した神澤篤啓氏、檜垣佑輔氏を始めとするバイオシグナリング研究室一同に感謝いたします。

資料(4)

Q J NUCL MED MOL IMAGING 2008;52:140-4

Non-standard radionuclide production for PET in Japan

Y. FUJIBAYASHI [1, 2], K. SUZUKI [2], T. FUKUMURA [2], T. MORI [1], S. KASAMATSU [1]

[1]*Biomedical Imaging Research Center University of Fukui, Fukui, Japan*
[2]*National Institute of Radiological Sciences Chiba, Japan*

There is a limited number of non-standard positron emission tomography (PET) radionuclides available in Japan. At the present time, non-standard PET nuclides (^{64}Cu and ^{62}Zn/^{62}Cu generator) are available from a medium energy cyclotron at the National Institute for Radiological Sciences in Chiba, Japan. Targetry for a small cyclotron has been installed on the cyclotrons of the University of Fukui. The production and distribution of these radionuclides from these cyclotrons will be described.

KEY WORDS: Radionuclide generators - Radiopharmaceuticals - Tomography, emission computed.

Although there are several medium and high energy cyclotrons in Japan, the majority of cyclotrons utilized for radionuclide productions are installed at commercial radiopharmaceutical companies (Nikon Medi Physics and Fuji-film RI Pharma) and are not utilized for the production of non-standard radionuclides. Interestingly, ^{123}I radiopharmaceuticals are available in Japan for routine clinical use and this radionuclide appears to be more readily available in Japan than in the United States. Only the AVF930 cyclotron at the National Institutes of Radiological Sciences (NIRS) (Chiba, Japan) is used to produce non-standard radionuclides for medical and other life sciences research. At the University of Fukui, we have developed targets on both the NKK super conducting cyclotron and the Siemens RDS cyclotron to produce ^{64}Cu. The target producing ^{64}Cu is currently being adapted to produce ^{77}Br. It should be noted that although there are over 100 small cyclotrons installed in Japan for the production of positron emission tomography (PET) radiopharmaceuticals, only the University of Fukui is actively involved in cyclotron research producing non-standard PET radionuclides.

Address reprint requests to: Y. Fujibayashi, Ph.D., D.Med.Sci., Biomedical Imaging Research Center, University of Fukui, 23-3, Shimoaizuki, Matsuoka, Eiheiji-cho, Yoshida, Fukui, 910-1193, Japan. E-mail: yfuji@fmsrsa.fukui-med.ac.jp

Production and distribution of ^{62}Zn/^{62}Cu generator at at the National Institutes of Radiological Sciences

Zinc-62 is routinely produced by the bombardment of a natural copper target with 18.6 MeV protons. The target system utilized is shown in Figure 1. After bombardment, the irradiated target is transferred to a hot cell using a monorail transport system and added to the ^{62}Zn purification system shown in Figure 2. The purified ^{62}Zn (yield >95% radionuclidic purity 3 h after bombardment) can be loaded on up to 4 cation exchange Sep-Pak plus Accell CM cartridges using the loading module shown schematically in Figure 3.[1] After the appropriate quality control the generators can be shipped up to 4 research institutions. Typical

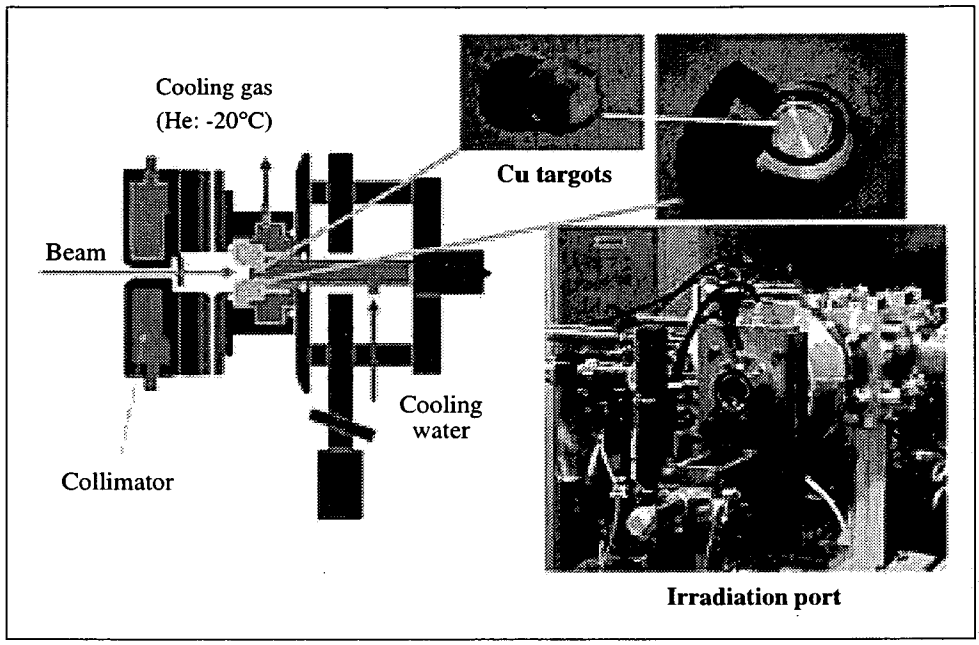

Figure 1.—Irradiation targets utilized on the AV AVF930 cyclotron at the National Institute for Radiological Sciences in Chiba, Japan.

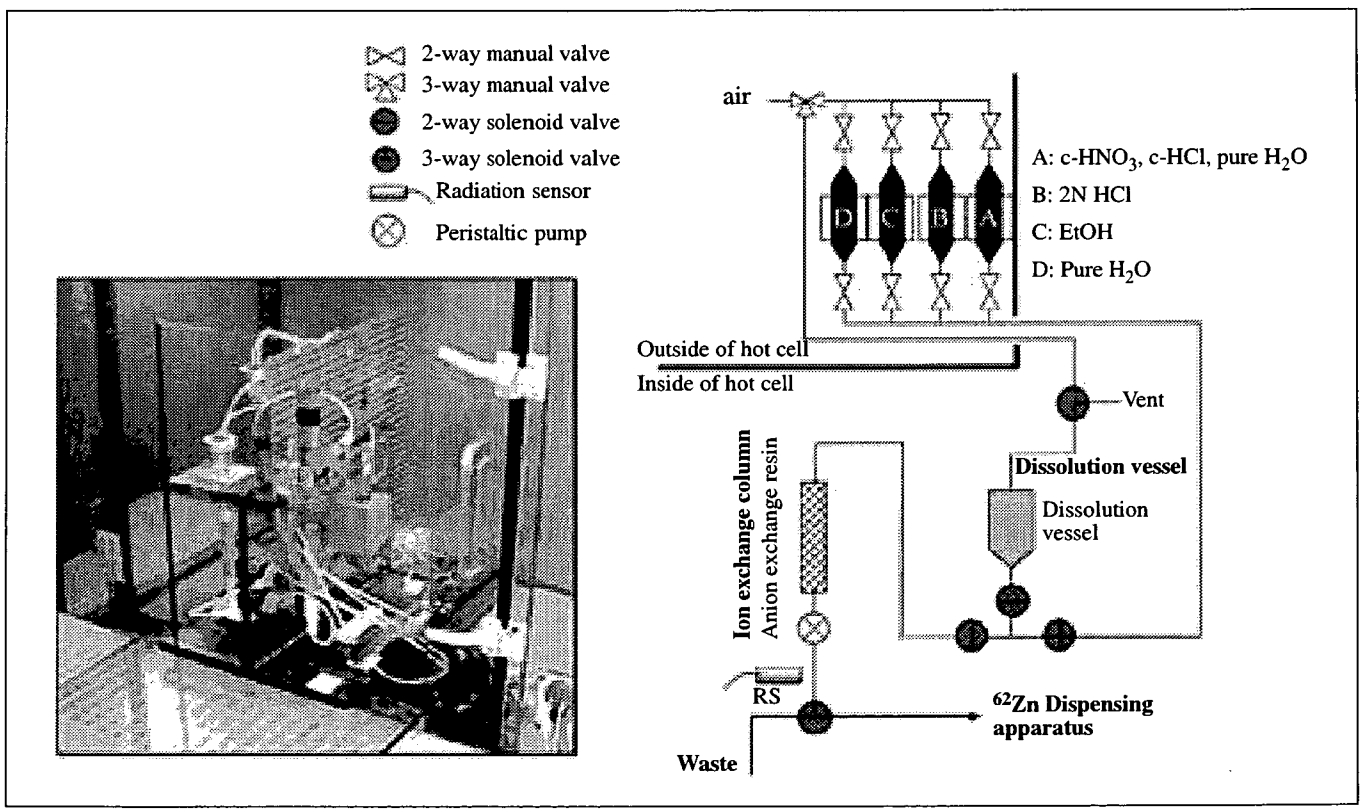

Figure 2.—System utilized for the separation of ^{62}Zn at the National Institute for Radiological Sciences cyclotron in Chiba, Japan.

資料 4

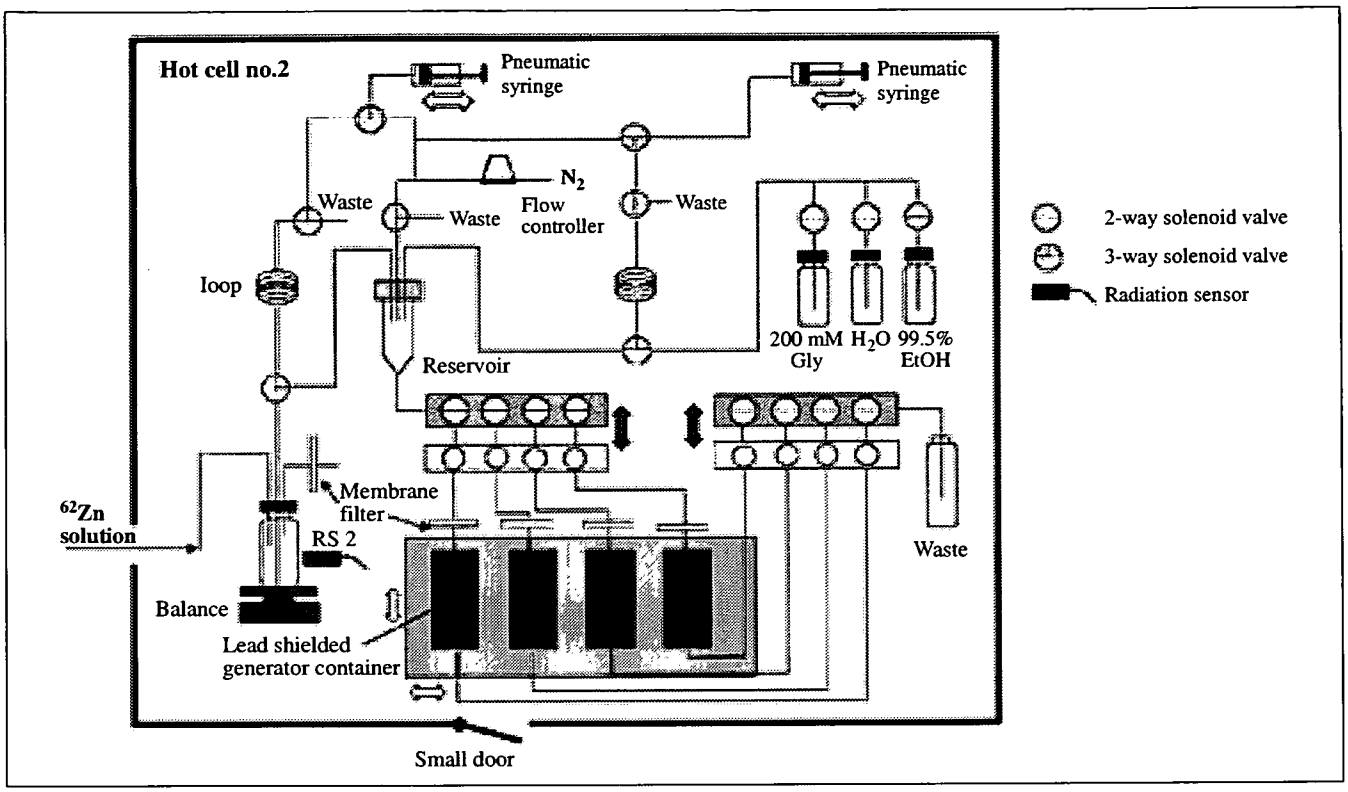

Figure 3.—Schematic of the system utilized to produce ^{62}Zn/^{62}Cu generators at the National Institute for Radiological Sciences in Chiba, Japan.

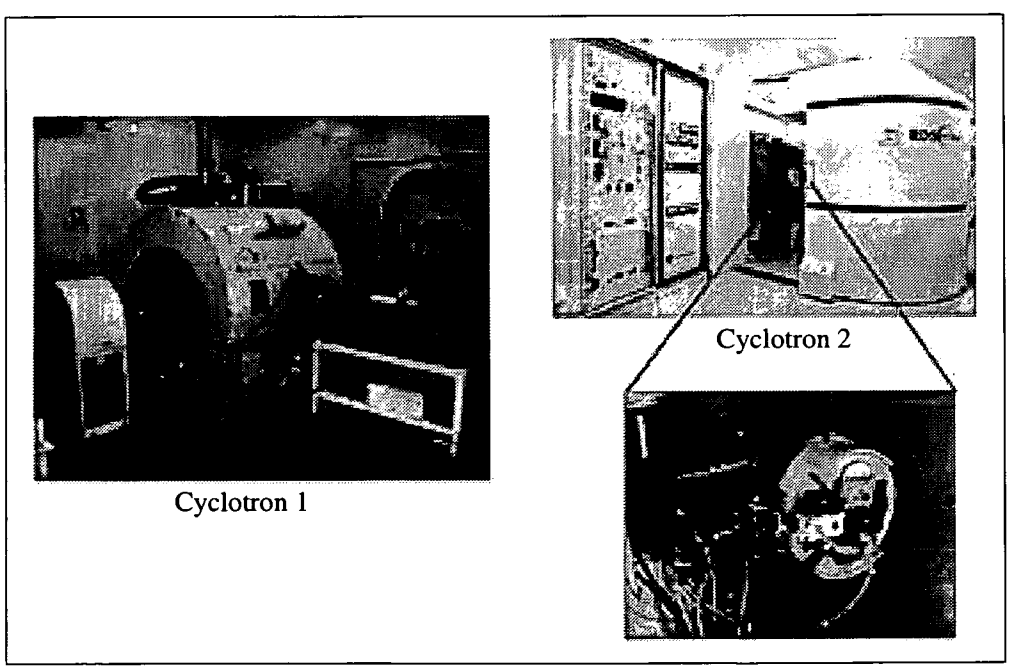

Figure 4.—Cyclotrons (JFE and Siemens RDS) utilized to produce non-standard radionuclides at the University of Fukui.

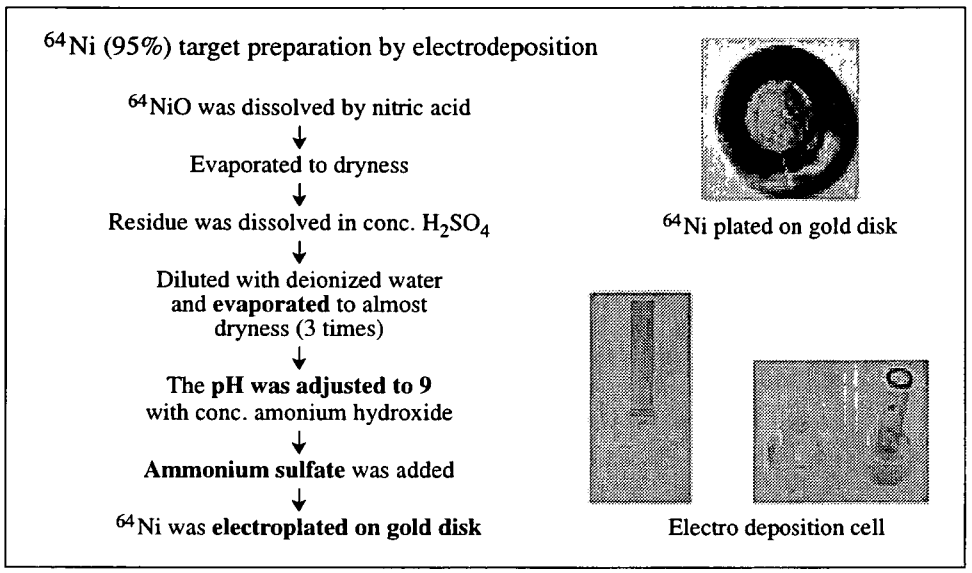

Figure 5.—Methodology used for the reparation of the enriched nickel target at the University of Fukui.

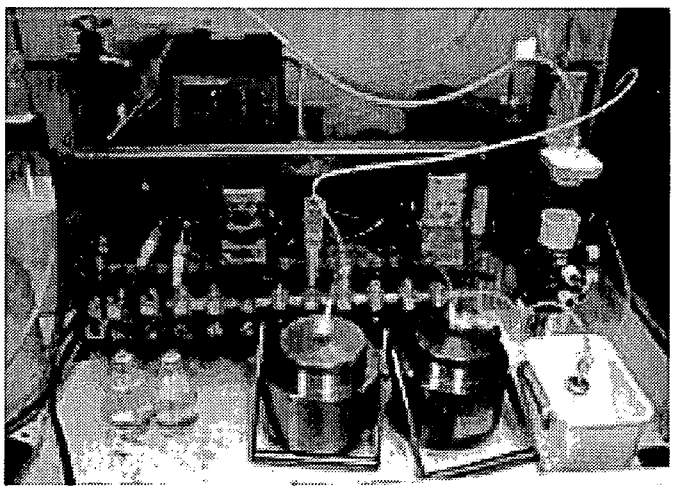

Figure 6.—Photograph of the purification system at the University of Fukui.

specifications for the generators are: generator activity (15 h post-end of bombardment [EOB]) 450-600 MBq; elution efficiency (^{62}Cu eluted) >90%; Cu^{2+} radionuclidic purity >99%; metal impurities present <0.2 ppm Cu^{2+}; <0.5% ppm; Zn^{2+}; Co^{2+}; Ni^{2+}. The generator eluate has been shown to be sterile and pyrogen free. The ^{62}Cu eluted from this generator is being utilized for research at several institutions including NIRS, The University of Fukui, Yokohama City University and the National Cancer Center at Kashiwa. Copper-62 ATSM has been studied in humans and the results published.[2]

Solid targets for positron emission tomography cyclotrons

Through a collaboration with the University of Fukui and Siemens (former CTI), a solid target system for self-shielded small cyclotrons has been developed (Figure 4). This target can be mounted inside the shield of the self-shielded cyclotron and the metal disk plated with the material to be irradiated automatically loaded and unloaded from the holder. A small tunnel has been installed under the cyclotron to allow the removal of the target.

In order to produce ^{64}Cu, ^{64}Ni is electroplated on a gold disk (Figure 5)[3] in a manner similar to that initially developed at Washington University in St. Louis, MO, USA.[4] After irradiation, the target disk is transferred to a hot cell containing an automated copper purification system (Figure 6) developed by the group at Fukui. This system consists of disposable syringes, valves, tubing and a preloaded ion exchange column, which allows the separation of the ^{64}Cu effectively and automatically. To date over 150 mCi of ^{64}Cu (100 μAh bombardment) has been prepared for basic research studies. The target system and separation system can, of course, be direct-

ly applied for the production of the other short-lived copper radionuclides, ^{60}Cu and ^{61}Cu.[5] The group at Fukui is currently developing copper selenide targets initially for the production of ^{77}Br and ultimately for the production of ^{76}Br.

Conclusions

At present, the non-standard PET radionuclides discussed in this issue of the *Quarterly Journal of Nuclear Medicine* have limited availability in Japan. The methodology production of these radionuclides both on medium energy cyclotrons, such as the one at NIRS, and on small PET cyclotrons, such as the one at Fukui, have been developed and are in use in these institutions. The research utilizing these radionuclides both in Japan and throughout the world showing the usefulness of these non-standard PET nuclides is increasing dramatically and we predict that more application of these nuclides both to basic and clinical research will be carried out in Japan.

References

1. Fukumura T, Okada K. Suzuki H, Nakao R, Mukai K, Szelecsenyi F *et al.* An improved Zn-62/Cu-62 generator based on a cation exchanger and its fully remote-controlled preparation for clinical use. Nucl Med Biol 2006;33:821-7.
2. Takahashi N, Fujibayashi Y, Yonekura Y, Welch MJ, Waki A, Tsuchida T *et al.* Copper-62 ATSM as a hypoxic tissue tracer in myocardial ischemia. Ann Nucl Med 2001;15:293-6.
3. Obata A, Kasamatsu S, McCarthy DW, Welch MJ, Saji H, Yonekura Y *et al.* Production of therapeutic quantity of Cu-64 using a 12 MeV cyclotron. Nucl Med Biol 2003;30:535-9.
4. McCarthy DW, Shefer RE, Klinkowstein RE, Bass LA, Margenau WH, Cutler CS *et al.* Efficient production of high specific activity ^{64}Cu using a biomedical cyclotron. Nucl Med Biol 1997;24:35-43.
5. McCarthy DW, Bass LA, Cutler PD, Shefer RE, Klinkowstein RE, Herrero P *et al.* High purity production and potential applications of copper-60 and copper-61. Nucl Med Biol 1999;26:351-8.

資料 4

資料(5)

資料 5

Available online at www.sciencedirect.com

ScienceDirect

Nuclear Medicine and Biology 33 (2006) 743–750

NUCLEAR MEDICINE — AND — BIOLOGY

www.elsevier.com/locate/nucmedbio

Double-tracer autoradiography with Cu-ATSM/FDG and immunohistochemical interpretation in four different mouse implanted tumor models

Takeshi Tanaka[a], Takako Furukawa[b], Shigeharu Fujieda[a], Shingo Kasamatsu[b], Yoshiharu Yonekura[b], Yasuhisa Fujibayashi[b,*]

[a]*Department of Otorhinolaryngology, University of Fukui, Matsuoka, Eiheiji-cho, Yoshida-gun, Fukui 910-1193, Japan*

[b]*Biomedical Imaging Research Center, University of Fukui, Matsuoka, Eiheiji-cho, Yoshida-gun, Fukui 910-1193, Japan*

Received 11 January 2006; received in revised form 10 May 2006; accepted 15 May 2006

Abstract

Background: We studied the regional characteristics within tumor masses using PET tracers and immunohistochemical methods.

Methods: The intratumoral distribution of ^{64}Cu-diacetyl-bis(N4-methylthiosemicarbazone) ([^{64}Cu]Cu-ATSM) and [^{18}F] 2-fluoro-2-deoxyglucose ([^{18}F]FDG) in mice with tumors of four different origins (LLC1, Meth-A, B16 and colon26) was compared with the immunohistochemical staining of proliferating cells (Ki67), blood vessels (CD34 or von Willebrand factor), and apoptotic cells (terminal deoxynucleotidyltransferase-mediated dUTP nick end labeling method).

Results: With all cell lines, [^{64}Cu]Cu-ATSM and [^{18}F]FDG were distributed with different gradation in the tumor mass. The immunohistochemical study demonstrated that the high [^{64}Cu]Cu-ATSM uptake regions were hypovascular and consisted of tumor cells arrested in the cell cycle, whereas the high [^{18}F]FDG uptake regions were hypervascular and consisted of proliferating cells.

Conclusion: In our study, it was revealed that one tumor mass contained two regions with different characteristics, which could be distinguished by [^{64}Cu]Cu-ATSM and [^{18}F]FDG. Because hypoxia and cell cycle arrest are critical factors to reduce tumor sensitivity to radiation and conventional chemotherapy, regions with such characteristics should be treated intensively as one of the primary targets. [^{64}Cu]Cu-ATSM, which can delineate hypoxic and cell cycle-arrested regions in tumors, may provide valuable information for cancer treatment as well as possibly for treating such regions directly as an internal radiotherapy reagent.

Keywords: Cu-ATSM; FDG; Hypoxia; Immunohistochemistry; Cancer imaging

1. Introduction

Tumor hypoxia is associated with resistance to radiotherapy and some chemotherapy. In addition, it increases tumor aggressiveness, metastatic potential, and angiogenesis, which lead to malignant progression [1,2]. Therefore, the detection of tumor hypoxia is important to predict tumor malignancy and to determine a medical treatment plan.

Cu-diacetyl-bis(N4-methylthiosemicarbazone) (Cu-ATSM) is reduced and trapped in cells under hypoxia, but not under normoxia. When labeled with a positron-emitting radioisotope of Cu, such as ^{60}Cu, ^{61}Cu, ^{62}Cu or ^{64}Cu, it works as a PET imaging agent to detect hypoxic tumors and hypoxic regions within a tumor mass [3–5]. [^{18}F] 2-Fluoro-2-deoxyglucose ([^{18}F]FDG) is widely used as a tracer of glucose uptake by tumors. Recent studies have indicated that [^{18}F]FDG uptake is increased in hypoxic cells in culture and in hypoxic regions within tumor xenografts [6–8]. This suggests the possibility that PET with [^{18}F]FDG could provide information about hypoxia in tumor and that the intratumoral distribution of [^{18}F]FDG and [^{64}Cu]Cu-ATSM might show some similarity. However, in our previous study, in which [^{64}Cu]Cu-ATSM and [^{18}F]FDG were coinjected into rabbits with a VX2 tumor, there was a significant difference between the intratumoral distribution of [^{64}Cu]Cu-ATSM and [^{18}F]FDG: [^{64}Cu]Cu-ATSM was highly accumulated at the edge of the tumor, whereas [^{18}F]FDG was highest inside the highest [^{64}Cu]Cu-ATSM region, although it was found in all areas [9]. This indicated that the uptake patterns of [^{64}Cu]Cu-ATSM and [^{18}F]FDG into tumor cells are different.

* Corresponding author. Tel.: +81 776 61 8491; fax: +81 776 61 8170.
E-mail addresses: wplants@mac.com (T. Tanaka), yfuji@fmsrsa.fukui-med.ac.jp (Y. Fujibayashi).

0969-8051/$ – see front matter © 2006 Elsevier Inc. All rights reserved.
doi:10.1016/j.nucmedbio.2006.05.005

In this study, we first verified whether the different intratumoral accumulation pattern of [^{64}Cu]Cu-ATSM and [^{18}F]FDG is a common phenomenon shared by different types of tumors. We selected four mouse tumor cell lines of quite different origin to make tumor masses and studied the intratumoral distribution of [^{64}Cu]Cu-ATSM and [^{18}F]FDG using similar methods to the previous study [9]. Second, we examined the tumors immunohistologically, focusing on microblood vessels and proliferating cells that represent the source of the supply and consumption of oxygen, respectively. The abundance of apoptotic cells, which has been reported to increase under hypoxia [10–12], was also examined. We compared regions with high [^{64}Cu]Cu-ATSM and [^{18}F]FDG uptake and revealed the relationship between the regional characteristics and accumulation of the two tracers.

2. Materials and methods

2.1. Tracers

^{64}Cu was produced on a small biomedical cyclotron at the Biomedical Imaging Research Center in the University of Fukui, Japan, according to a published method [13]. [^{64}Cu]Cu-ATSM was synthesized by mixing 200-mM glycine buffer containing ^{64}Cu and H_2 ATSM in dimethly sulfoxide (1:100 by molar ration), as described previously [3]. The radiochemical purity of synthesized [^{64}Cu]Cu-ATSM was >99%, evaluated by HPLC (LC-10ADVP; Shimadzu, Kyoto, Japan) using a reversed phase column (Cosmosil 5C18-AR, 4.6×50 mm+4.6×150 mm; Nacalai Tesque, Kyoto, Japan) [14]. [^{18}F]FDG was synthesized by the method of Hamacher et al. [15] with an automated [^{18}F] FDG synthesizing system (JFE, Tokyo, Japan). The specific activity of [^{64}Cu]Cu-ATSM was 56 GBq/μmol, and that of [^{18}F]FDG was 20 to 50 GBq/μmol.

2.2. Animal models

Mice were treated in accordance with the animal treatment regulations of the University of Fukui throughout the experiments. The four mouse tumor cell lines used were B16 (melanoma), Meth-A (sarcoma), colon26 (adenocarcinoma) and LLC1 (Lewis lung carcinoma). Male mice, C57BL/6 and BALB/C, were obtained from Japan SLC (Shizuoka, Japan) at 6 weeks old and 20 to 25 g of body weight. The tumor cells, approximately 1×10^7 cells suspended in PBS, were injected into the hypodermis. B16 and LLC1 were implanted into C57BL/6, and Meth-A and colon26 into BALB/C mice. Three mice per cell line were prepared.

2.3. Autoradiography

At 4 weeks after the implantation of tumor cells, each mouse was injected intravenously with 74 MBq (2 mCi) [^{18}F]FDG and 0.37 MBq (10 μCi) [^{64}Cu]Cu-ATSM. Sixty minutes after the injection, the mice were sacrificed and the tumors were removed. The removed tumors were immediately covered with optimal cutting temperature (OCT) compound and frozen in methanol cooled with dry ice. They were divided into sections, and the cutting surfaces were flattened using a cryostat (Cryocut 1800, Leica, Wetzlar, Germany), then subjected to dual-tracer autoradiography [4]. [^{18}F]FDG images were acquired over 3 min, exposing the frozen sections to an imaging plate (BAS-MP 2040S; Fuji Photo Films, Japan) in a freezer. The imaging plate was scanned with a bioimaging analyzer (BAS-1500; Fuji Photo Films). After waiting 40 h for ^{18}F decay, [^{64}Cu]Cu-ATSM images were acquired over 45 h and the imaging plate was scanned. The distributions of [^{18}F]FDG and [^{64}Cu]Cu-ATSM were visualized by Mac-BAS v2.52 software (Fuji Photo Film). The contribution of ^{64}Cu radioactivity to the FDG image (the first autoradiography) was estimated to be around 1%, and the contribution of ^{18}F radioactivity to the Cu-ATSM image (the second exposure) was less than 0.1%. In each tumor section, the highest photostimulated luminescence region was classified as 100%, and the background was 0%. The 0% to 100% range was divided into four parts and colored red (75–100%), orange (50–75%), green (25–50%) and blue (0–25%), and the background was black. The colored image was saved in true color TIFF format.

2.4. Immunohistochemical staining

The frozen blocks used for the double tracer autoradiography were thawed, fixed in 10% neutral-buffered formalin and embedded in paraffin. The sections used for the immunohistochemical staining were made from the region within 50 μm from the surface exposed for autoradiography. After ^{64}Cu decay, immunohistochemical staining was carried out to detect proliferating cells, blood vessels and apoptotic cells using 2-μm-thick serial paraffin sections.

2.4.1. Proliferating cells

Ki67 is a nuclear protein expressed at all active phases of the cell cycle (G_1, S, G_2 and mitosis) with the highest expression in the G_2/M phase, but it is absent from the resting cells (G_0). The proliferating cell fraction can be determined immunohistochemically by using antibodies against Ki67 [16]. The sections were deparaffinized and rehydrated to detect proliferating cells, then endogenous peroxidase was blocked by 3% hydrogen peroxide. Antigen retrieval was carried out by microwaving for 25 min in 10-mM citrate buffer at pH 6. Nonspecific stain-blocking reagent (X0909, Dako Cytomation, Glostrup, Denmark) was applied for 20 min at room temperature (RT). The sections were then incubated overnight at 4°C with rat monoclonal antimouse Ki67 antigen antibody (M7249, Dako Cytomation) in 1:50 dilution with PBS. After washing with PBS, the sections were incubated with rabbit antirat biotinylated secondary antibody (E0468, Dako Cytomation) in 1:200 dilution with PBS for 30 min at RT, then incubated with streptavidin conjugated to horseradish peroxidase (streptavidin-HRP, K0673, Dako Cytomation) for 30 min at RT. Finally, the sections were incubated with 3,3′ -diaminobenzine tetrahydrochloride

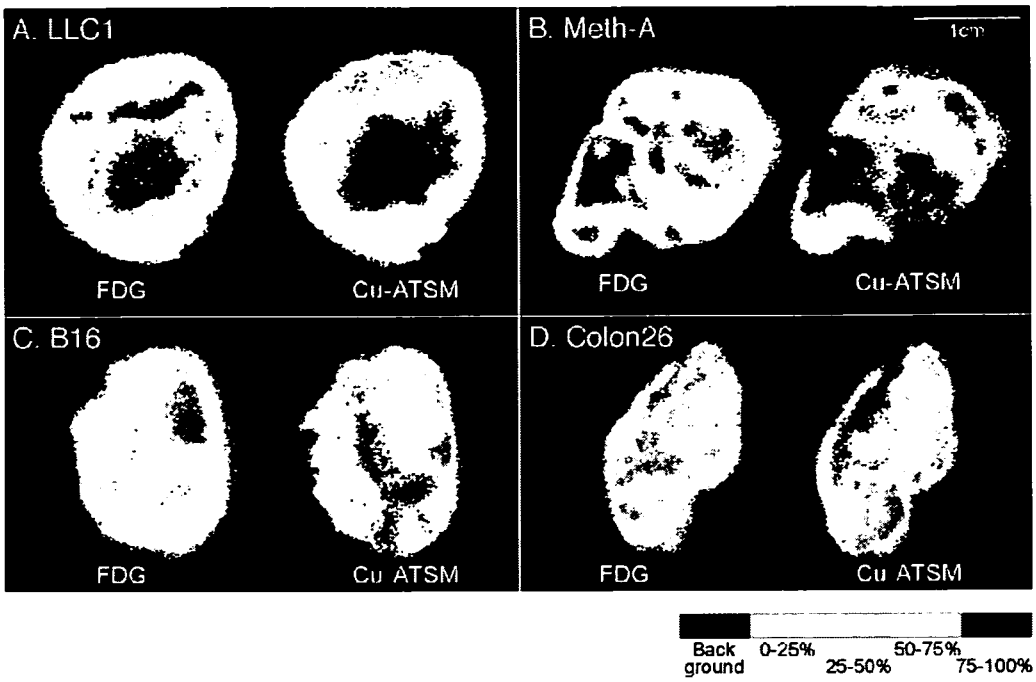

Fig. 1. Representative intratumoral distributions of ^{18}FDG and ^{64}Cu-ATSM in the tumor mass of LLC1(A), Meth-A(B), B16(C) and colon26(D) are shown. Autoradiographic images of ^{18}FDG and ^{64}Cu-ATSM were made from the same section.

solution (DAB Liquid System, Dako Cytomation) until suitable staining developed, then the nuclei were slightly counterstained with hematoxylin.

2.4.2. Blood vessels

CD34 is a cell glycoprotein expressed in the endothelial cells of small blood vessels [17]. To detect blood vessels in the sections, we used anti-CD34 antibody for B16 and colon26 tumors. The sections were deparaffinized and rehydrated, and endogenous peroxidase was blocked as described above. Antigen retrieval was performed for 15 min, and nonspecific staining was blocked as above. The sections were then incubated overnight at 4°C with rat antimouse CD34 antibody (HM1015; Hycult Biotechnology, Netherlands) in 1:20 dilution with PBS. After washing with PBS, the sections were incubated with rabbit antirat biotinylated secondary antibody (Dako Cytomation) in 1:100 dilution with PBS for 30 min at RT, and then incubated with streptavidin-HRP for 30 min at RT. The detection of peroxidase activity and the counterstaining were performed as described above.

von Willebrand factor (vWF) is synthesized by endothelial cells [18] and used for blood vessel staining. Because the anti-CD34 antibody did not work with Meth-A and LLC1 tumor sections because of high background staining, we used anti-vWF antibody for microvessel staining with Meth-A and LLC1 tumors. The sections were treated as described for CD34 staining, then incubated overnight at 4°C with polyclonal rabbit antimouse vWF antibody (A0082, Dako Cytomation) in 1:500 dilution with PBS. After washing with PBS, the sections were incubated with goat antirabbit immunoglobulin conjugated to peroxidase-labeled dextran polymer (Dako EnVision+, K4002, Dako Cytomation) for 30 min at RT. The peroxidase activity and the counterstaining were detected as described above.

2.4.3. Apoptotic cells

To evaluate apoptosis, we used a commercially available kit (ApopTag Peroxidase Kit, S7100; Chemicon, Temecula, CA), which uses the terminal deoxynucleotidyltransferase (TdT)-mediated dUTP nick end labeling method [19]. Briefly, after sections were deparaffinized and rehydrated, and endogenous peroxidase was blocked by 3% hydrogen peroxide, the sections were incubated with proteinase K (Wako, Japan) in 1:50000 dilution with PBS for 30 min at 30°C. After rinsing with PBS, the sections were incubated with equilibration buffer at RT for 13 min, then with TdT enzyme and reaction buffer, and mixed at a 3:7 ratio, at 37°C for 60 min. The sections were then steeped in stop–wash buffer, prepared at 1:35 dilution with PBS, at 37°C for 30 min. After washing with PBS, the sections were incubated with anti-digoxigenin-peroxidase at RT for 30 min. Peroxidase activity and counterstaining were detected as described above.

2.5. Image analysis

Whole images of the serial sections stained for Ki67, CD34, vWF and apoptosis were captured by a scanner (Epson GT-8500) and saved in JPEG format. Composite images were made using Adobe Photoshop to compare the autoradiographic images with those of the stained sections. [^{64}Cu]Cu-ATSM and [^{18}F]FDG images were stacked in layers above the images of stained sections and made translucent. A composite image was made for each tumor

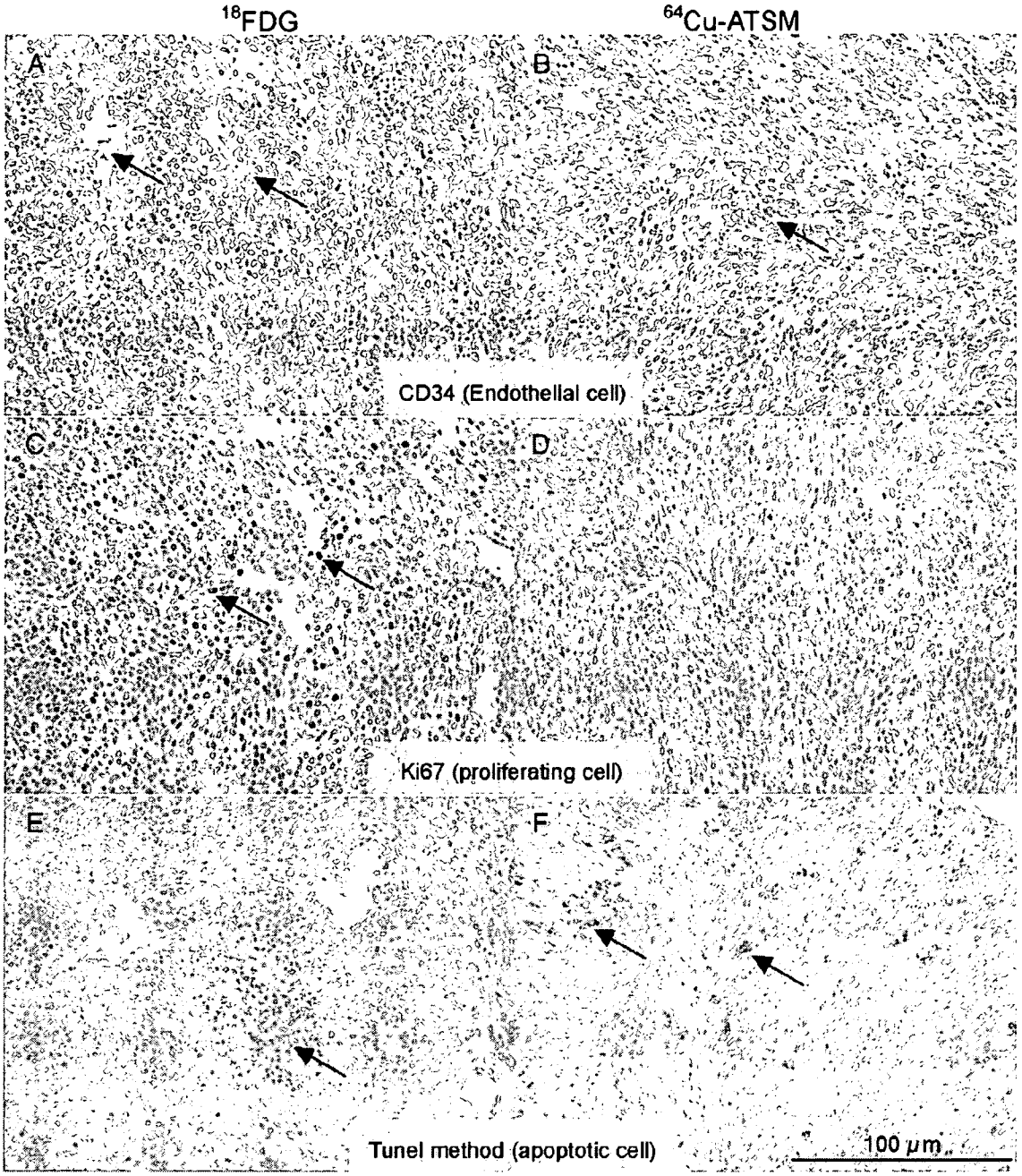

Fig. 2. Examples of immunohistochemical staining for CD34 (A, B), Ki67 (C, D) and Tunel (E, F) in colon26 sections at ×200. Panels A, C and E show regions with the highest ^{18}FDG accumulation. Panels B, D and F show regions with the highest ^{64}Cu-ATSM accumulation. Arrows indicate blood vessels (13 vessels) in panel A; single endothelial cells, which do not constitute the vessel, in panel B; and proliferating cells (198 cells) in panel C. Few proliferating cells (0 cells) are seen in D. In E, the arrow indicates necrosis. Few apoptotic cells are seen in E. In F, arrows indicate apoptotic cells (50 cells).

mass, and three composite images were quantified for each cell line. In each composite image, three areas from the region of each color for [^{64}Cu]Cu-ATSM and [^{18}F]FDG were analyzed. Digital images of the area (0.31 mm^2) were obtained at ×200 magnification using a microscope (Olympus BX50) mounted with a CCD camera and connected to a Windows computer. Proliferating cells, microblood vessels and apoptotic cells were counted manually on the computer monitor. The numbers of positively stained cells or microvessels in the nine areas (three areas from one section, one section from one mouse and three mice for one tumor cell line) were averaged for each different color indication level of [^{64}Cu]Cu-ATSM and [^{18}F]FDG accumulation.

2.6. Statistical analysis

Statistical analyses were performed with StatView software, Version 5.0. For comparison, the determination of correlation coefficients and the Mann–Whitney U test were applied. $P < .05$ was considered as statistically significant.

3. Results

3.1. Intratumoral distribution of [^{18}F]FDG and [^{64}Cu]Cu-ATSM

To analyze the intratumoral distribution of [^{18}F]FDG and [^{64}Cu]Cu-ATSM, we performed dual autoradiography with implanted mouse tumors of different origins. The representative images are shown in Fig. 1. [^{64}Cu]Cu-ATSM mainly accumulated at the edge of the tumors, and no accumulation was seen in the center where the cells were necrotic. On the other hand, the highest uptake region of [^{18}F]FDG was seen inner adjacent to that of [^{64}Cu]Cu-ATSM. The highest regions of [^{18}F]FDG and [^{64}Cu]Cu-ATSM, colored red, were distributed differently in all sections studied.

3.2. Microvessel density

To assess microvessel density (MVD), we counted the number of blood vessels per view in each region differentially colored according to the tracer accumulation. In the highest [^{18}F]FDG regions, abundant vessels were spreading into the tumor tissue and seemed to be functioning as blood vessels (Fig. 2A). Tumor cells near the vessels contained large and round nuclei, but small necrotic regions were frequently observed some distance from the blood vessels.

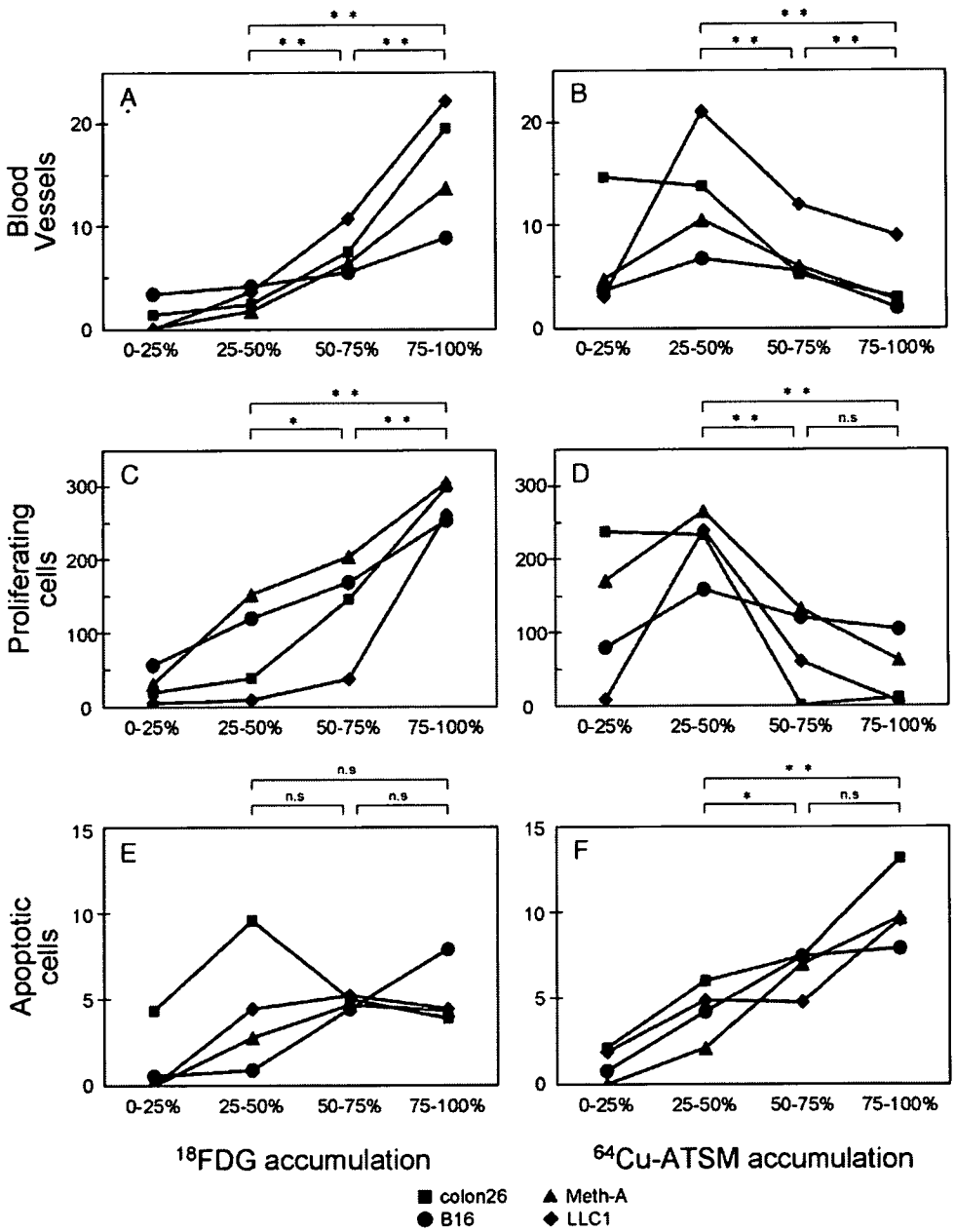

Fig. 3. These graphs show the number of blood vessels, proliferating cells and apoptotic cells compared with the intratumoral distribution of ^{18}FDG/^{64}Cu-ATSM. Three tumor sections were quantified for each cell line. Each point represents the average of positively stained cells in nine views from each region classified by the degree of ^{18}FDG or ^{64}Cu-ATSM accumulation. There were approximately 2000 tumor cells in the microscope view. Statistical analyses were performed by summarizing four cell lines (**$P < .01$, *$P < .05$, ns indicates not significant).

The vessel count in the highest uptake region of [^{64}Cu]Cu-ATSM was remarkably less than that of [^{18}F]FDG, but there was no necrosis, and abundant viable tumor cells were seen (Fig. 2B). The tumor cells in the highest [^{64}Cu]Cu-ATSM region had smaller nuclei and lower chromatin concentration compared with the highest [^{18}F]FDG region.

The relationship between MVD and the accumulation of two tracers in each tumor mass are shown in Fig. 3A and B, in which each point represents the mean of nine blood vessel counts from each region. Each graph summarizes the data of 144 views in 48 regions from 12 tumor sections. Positive correlation was found between [^{18}F]FDG and MVD in all four tumor cell lines (Fig. 3A). On the other hand, the number of vessels decreased with the increase in [^{64}Cu]Cu-ATSM uptake, excluding the lowest [^{64}Cu]Cu-ATSM uptake region (Fig. 3B). In all cell lines except colon26, the MVD was very low in the lowest [^{64}Cu]Cu-ATSM region, where most tumor cells were necrotic with a shrunken nucleus. For colon26, MVD was relatively high compared with the other tumors in the lowest [^{64}Cu]Cu-ATSM region, which contained abundant blood vessels and viable tumor cells.

3.3. Cell proliferation

To evaluate cell proliferation in each section, we performed Ki67 immunohistochemistry. Positive nuclear staining of Ki67 in tumor cells was abundantly observed in the highest [^{18}F]FDG region, but it was hardly observed in that of [^{64}Cu]Cu-ATSM (Fig. 2C and D). Similar to MVD, the number of Ki67 positive cells increased with [^{18}F]FDG uptake (Fig. 3C) and decreased with [^{64}Cu]Cu-ATSM uptake (Fig. 3D). Cell proliferation was active in the lowest [^{64}Cu]Cu-ATSM region only in the colon26 sections.

3.4. Apoptosis

To assess apoptosis, we used an ApopTag Peroxidase Kit to stain the sections, and the number of apoptotic cells was counted. In the highest [^{18}F]FDG region, few apoptotic cells were observed (Fig. 2E). The regions in which tumor cells with shrunken nuclei gathered were not stained, indicating that the regions were necrotic, not apoptotic. In the highest uptake region of [^{64}Cu]Cu-ATSM, more apoptotic cells were seen compared with the [^{18}F]FDG region (Fig. 2F), although the number of apoptotic cells was less than 1% of all tumor cells. A positive correlation was found between the apoptotic cell number and [^{64}Cu]Cu-ATSM accumulation (Fig. 3F), but no correlation was found between the apoptotic cell number and [^{18}F]FDG accumulation (Fig. 3E).

4. Discussion

In this study, we demonstrated that [^{64}Cu]Cu-ATSM and [^{18}F]FDG were distributed with different gradation of the tumor mass from all four mouse tumor cell lines (Fig. 1). At the macroscopic level, the tumor cells of LLC1 and colon26 formed a concentric circular shape around the necrosis, with the highest [^{64}Cu]Cu-ATSM uptake seen in the outer region and the highest [^{18}F]FDG uptake in the inner region of the sections (Fig. 1A and D). On the other hand, with Meth-A and B16, the tumor cells tended to form multiple tubercular shapes when the tumor size increased and the section diameter exceeded 2 cm. In these sections, [^{64}Cu]Cu-ATSM was found at highest in the outer region of the tubercles, and [^{18}F]FDG was found at highest in the inner region of the tubercles bordering the region accumulating [^{64}Cu]Cu-ATSM (Fig. 1B and C). Thus, it seemed to be a phenomenon shared by various tumors that [^{18}F]FDG and [^{64}Cu]Cu-ATSM were accumulated with different gradation, forming a unique pattern of a high [^{64}Cu]Cu-ATSM region surrounding a high [^{18}F]FDG region within a tumor mass.

In the high [^{18}F]FDG region, MVD was high and abundant proliferating cells were observed (Fig. 2A and C). A positive correlation was found between [^{18}F]FDG accumulation and the number of proliferating cells (Fig. 3A). The high [^{18}F]FDG regions seemed to be under normal oxygen tension, because MVD was quite high and [^{64}Cu]Cu-ATSM, a hypoxic marker, did not accumulate in these regions. These findings indicate that [^{18}F]FDG was mainly taken up by proliferating tumor cells, which are not so hypoxic that [^{64}Cu]Cu-ATSM will accumulate. In these regions, cell death was mainly from necrosis, which could be caused by environmental aggravation. Because of the abnormality of tumor vasculature and very active cell proliferation, severe disturbance to the microcirculation and oxygen supply would occur, leading to tumor cell death at some distance from the vessels. Tumor cells in the high [^{18}F]FDG region seemed to have characteristics specific to malignant tumors, in which tumor cells proliferate without limit until they die. However, there are data by Pugachev et al. [20] that suggest that the higher FDG uptake was indicative of tumor hypoxia, but neither blood flow nor cellular proliferation, with the nude mice bearing Dunning prostate tumor. There are also several articles supporting the positive correlation between FDG uptake and blood flow in experimental and clinical settings [21–23]. The discrepancy can be resulted from the difference in the tumor types, difference in the techniques to evaluate the vascularity or blood flow (perfusion by Hoechst, microvessel density and O-15 H_2O, etc.), difference in the resolution of the images or difference in some other conditions.

In the highest [^{64}Cu]Cu-ATSM regions, MVD was very low and few proliferating cells were observed (Fig. 2B and D). A negative correlation was found between MVD and [^{64}Cu]Cu-ATSM accumulation (Fig. 3B), in agreement with the hypothesis that [^{64}Cu]Cu-ATSM accumulates in hypoxic regions. These regions had few necrotic cells and mostly consisted of viable tumor cells whose nuclei were uniform but smaller than those found in the highest [^{18}F]FDG regions. It has been reported that some tumor cells survive hypoxia in environmental aggravation but are arrested in the G_0 or G_1 phase [24,25]. There seem to be similarities between surviving tumor cells and cells in the

highest [^{64}Cu]Cu-ATSM region. The high [^{64}Cu]Cu-ATSM region can be described as hypovascular, and the cell cycle-arrested region is where oxygen consumption and glucose metabolism are reduced and tumor cells quietly wait for the environment to improve. In addition, a positive correlation was found between [^{64}Cu]Cu-ATSM accumulation and the number of apoptotic cells (Fig. 3F). It should be noted that the number of apoptotic cells in the highest [^{64}Cu]Cu-ATSM region, even where apoptotic cells were most frequently observed, was less than 1% of all tumor cells, although it was reported that hypoxia can induce apoptotic cell death in tumor cells [10–12]. Tumor cells in the high [^{64}Cu]Cu-ATSM region seem to have atypical characteristics similar to malignant tumors: they can maintain self-control. They respond to environmental changes and stop cell proliferation, and when they die, they die of apoptosis, a programmed cell death.

In our study, it was revealed that there are regions containing cells of different phenotypes in the same tumor mass, which can be distinguished using PET tracers [^{18}F]FDG and [^{64}Cu]Cu-ATSM. As the tumor mass is formed by cells from a single cell line, different phenotypes should have resulted from adaptation to the intratumoral microenvironment, such as hypoxia and malnutrition. Radiotherapy and some chemotherapy are effective in malignant tumors against normoxic and actively dividing cells, but are less effective against cells with low oxygen tension and arrested cell cycle [26,27]. Our study implies that tumor cells in the high [^{18}F]FDG region are sensitive to therapy, but those in the high [^{64}Cu]Cu-ATSM region are resistant.

It was also interesting that lone endothelial cells were often detected in the highest [^{64}Cu]Cu-ATSM regions (Fig. 2B). Hypoxia induces angiogenic factors such as vascular endothelial growth factor and platelet-derived endothelial cell growth factor [28,29]. If endothelial cells grow and form functional blood vessels, the environment in this region will be improved and tumor cells may start to proliferate. It has been reported that, after reoxygenation, tumor cells adapting to chronic hypoxia resume cell cycle progression with acquired resistance against radiation and anticancer drugs [30–32]. Tumor cells in the high [^{64}Cu]Cu-ATSM region are highly likely to turn into such death-resistant cells.

Our study indicated that the high [^{18}F]FDG region is where tumor cells actively proliferate and should receive immediate anticancer treatment, whereas the high [^{64}Cu]Cu-ATSM region is likely to be less sensitive to conventional antitumor treatment and needs more intensive and aggressive therapy. In a clinical PET study with [^{60}Cu]Cu-ATSM, tumors with high [^{60}Cu]Cu-ATSM accumulation responded poorly to therapy, and such tumors tended to develop local recurrence and lymph node metastasis [33,34]. Those reports confirm the ability of [^{60}Cu]Cu-ATSM PET to predict the tumor response to therapy and the prognosis, and support our view that the high Cu-ATSM region responds poorly to conventional therapy and needs aggressive treatment. As an intensive radiotherapy to the hypoxic region, hypoxia imaging (Cu-ATSM)-guided intensity-modulated radiation therapy has been performed for head-and-neck cancer patients [35]. Higher doses of radiation to the hypoxic region can overcome hypoxic resistance and increase the anticancer effect with minimal normal tissue complications.

Cu-ATSM itself has potential as an internal radiotherapy agent directly targeting such hypoxic and cell cycle-arrested regions when labeled with β^--emitting radioisotopes such as ^{64}Cu or ^{67}Cu. In animal models with a tumor, [^{64}Cu]Cu-ATSM could improve the survival time without acute toxicity [36,37]. When a sufficient radiation dose of [^{64}Cu]Cu-ATSM was taken up into the tumor cells, apoptotic cell death was induced because of DNA damage by radiation from ^{64}Cu inside the cells [38]. Because the β^- particle, the main cytotoxic agent of ^{64}Cu, penetrates tissue to several hundred micrometers, the cytotoxic effect of ^{64}Cu expands to neighboring cells, which will increase the anticancer effect.

5. Conclusion

Both [^{18}F]FDG and [^{64}Cu]Cu-ATSM provide important information about tumors, although the accumulation of each tracer indicates different characteristics of the tumor tissue. Information on the regional characteristics of tumors by [^{64}Cu]Cu-ATSM and [^{18}F]FDG PET will enable us to make finely tuned and effective treatment plans for tumors, especially when they are hypoxic and resistant to conventional therapy.

Acknowledgments

This study was partly supported by KAKENHI, a grant-in-aid for Scientific Research from the Ministry of Education, Culture, Sports, Science and Technology (MEXT) Japan, a 21st Century COE program "Biomedical Imaging Technology Integration Program" from Japan Society of the Promotion of Science (JSPS) and the Research and Development Project Aimed at Economic Revitalization (Leading Project) "Research and Development of Technology for Measuring Vital Functions Merged with Optical Technology" from MEXT Japan.

References

[1] Pitson G, Fyles A, Milosevic M, Wylie J, Pintilie M, Hill R. Tumor size and oxygenation are independent predictors of nodal diseases in patients with cervix cancer. Int J Radiat Oncol Biol Phys 2001;51: 699–703.
[2] Brown JM. The hypoxic cell: a target for selective cancer therapy — eighteenth Bruce F. Cain Memorial Award lecture. Cancer Res 1999;59:5863–70.
[3] Fujibayashi Y, Taniuchi H, Yonekura Y, Ohtani H, Konishi J, Yokoyama A. Copper-62-ATSM: a new hypoxia imaging agent with high membrane permeability and low redox potential. J Nucl Med 1997;38:1155–60.

[4] Fujibayashi Y, Cutler CS, Anderson CJ, et al. Comparative studies of Cu-64-ATSM and C-11-acetate in an acute myocardial infarction model: ex vivo imaging of hypoxia in rats. Nucl Med Biol 1999;26: 117–21.
[5] O'donoghue JA, Zanzonico P, Pugachev A, et al. Assessment of regional tumor hypoxia using (18)F-fluoromisonidazole and (64)Cu(II)-diacetyl-bis(N4-methylthiosemicarbazone) positron emission tomography: comparative study featuring microPET imaging, Po(2) probe measurement, autoradiography, and fluorescent microscopy in the R3327-AT and FaDu rat tumor models. Int J Radiat Oncol Biol Phys 2005;61:1493–502.
[6] Burgman P, Odonoghue JA, Humm JL, Ling CC. Hypoxia-Induced increase in FDG uptake in MCF7 cells. J Nucl Med 2001;42:170–5.
[7] Dearling JL, Flynn AA, Sutcliffe-Goulden J, et al. Analysis of the regional uptake of radiolabeled deoxyglucose analogs in human tumor xenografts. J Nucl Med 2004;45:101–7.
[8] Zhao S, Kuge Y, Mochizuki T, Takahashi T, et al. Biologic correlates of intratumoral heterogeneity in 18F-FDG distribution with regional expression of glucose transporters and hexokinase-II in experimental tumor. J Nucl Med 2005;46:675–82.
[9] Obata A, Yoshimoto M, Kasamatsu S, et al. Intra-tumoral distribution of (64)Cu-ATSM: a comparison study with FDG. Nucl Med Biol 2003;30:529–34.
[10] Graeber TG, Osmanian C, Jacks T, et al. Hypoxia-mediated selection of cells with diminished apoptotic potential in solid tumours. Nature 1996;379:88–91.
[11] Nagarajah NS, Vigneswaran N, Zacharias W. Hypoxia-mediated apoptosis in oral carcinoma cells occurs via two independent pathways. Mol Cancer 2004;3:38.
[12] Pan Y, Oprysko PR, Asham AM, Koch CJ, Simon MC. p53 cannot be induced by hypoxia alone but responds to the hypoxic microenvironment. Oncogene 2004;23:4975–83.
[13] Obata A, Kasamatsu S, McCarthy DW, et al. Production of therapeutic quantities of (64)Cu using a 12 MeV cyclotron. Nucl Med Biol 2003; 30:535–9.
[14] Obata A, Yoshimi E, Waki A, et al. Retention mechanism of hypoxia selective nuclear imaging/radiotherapeutic agent Cu-diacetyl-bis(N4-methylthiosemicarbazone) (Cu-ATSM) in tumor cells. Ann Nucl Med 2001;15:499–504.
[15] Hamacher K, Coenen HH, Stocklin G. Efficient stereospecific synthesis of no-carrier-added 2-[18F]-fluoro-2-deoxy-D-glucose using aminopolyether supported nucleophilic substitution. J Nucl Med 1986;27:235–8.
[16] Scholzen T, Gerdes J. The Ki-67 protein: from the known and the unknown. J Cell Physiol 2000;182:311–22.
[17] Fujieda S, Sunaga H, Tsuzuki H, Tanaka N, Saito H. Expression of platelet-derived endothelial cell growth factor in oral and oropharyngeal carcinoma. Clin Cancer Res 1998;4:1583–90.
[18] Sporn LA, Chavin SI, Marder VJ, Wagner DD. Biosynthesis of von Willebrand protein by human megakaryocytes. J Clin Invest 1985; 76:1102–6.
[19] Fujieda S, Inuzuka M, Tanaka N, et al. Expression of p27 is associated with Bax expression and spontaneous apoptosis in oral and oropharyngeal carcinoma. Int J Cancer 1999;84:315–20.
[20] Pugachev A, Ruan S, Carlin S, et al. Dependence of FDG uptake on tumor microenvironment. Int J Radiat Oncol Biol Phys 2005;62: 545–53.
[21] Bos R, van Der Hoeven JJ, van Der Wall E, et al. Biologic correlates of (18)fluorodeoxyglucose uptake in human breast cancer measured by positron emission tomography. J Clin Oncol 2002;20: 379–87.
[22] Zasadny KR, Tatsumi M, Wahl RL. FDG metabolism and uptake versus blood flow in women with untreated primary breast cancers. Eur J Nucl Med Mol Imaging 2003;30:274–80.
[23] Schroeder T, Yuan H, Viglianti BL, et al. Spatial heterogeneity and oxygen dependence of glucose consumption in R3230Ac and fibrosarcomas of the Fischer 344 rat. Cancer Res 2005;65: 5163–71.
[24] Amellem O, Sandvik JA, Stokke T, Pettersen EO. The retinoblastoma protein-associated cell cycle arrest in S-phase under moderate hypoxia is disrupted in cells expressing HPV18 E7 oncoprotein. Br J Cancer 1998;77:862–72.
[25] Webster L, Hodgkiss RJ, Wilson GD. Cell cycle distribution of hypoxia and progression of hypoxic tumour cells in vivo. Br J Cancer 1998;77:227–34.
[26] Cuisnier O, Serduc R, Lavieille JP, Longuet M, Reyt E, Riva C. Chronic hypoxia protects against gamma-irradiation-induced apoptosis by inducing bcl-2 up-regulation and inhibiting mitochondrial translocation and conformational change of bax protein. Int J Oncol 2003;23:1033–41.
[27] Yokoi K, Fidler IJ. Hypoxia increases resistance of human pancreatic cancer cells to apoptosis induced by gemcitabine. Clin Cancer Res 2004;10:2299–306.
[28] Koong AC, Denko NC, Hudson KM, et al. Candidate genes for the hypoxic tumor phenotype. Cancer Res 2000;60:883–7.
[29] Sipos B, Weber D, Ungefroren H, et al. Vascular endothelial growth factor mediated angiogenic potential of pancreatic ductal carcinomas enhanced by hypoxia: an in vitro and in vivo study. Int J Cancer 2002;102:592–600.
[30] Kinoshita M, Johnson DL, Shatney CH, Lee YL, Mochizuki H. Cancer cells surviving hypoxia obtain hypoxia resistance and maintain anti-apoptotic potential under reoxygenation. Int J Cancer 2001;91: 322–6.
[31] Koritzinsky M, Wouters BG, Amellem O, Pettersen EO. Cell cycle progression and radiation survival following prolonged hypoxia and re-oxygenation. Int J Radiat Biol 2001;77:319–28.
[32] Dong Z, Wang J. Hypoxia selection of death-resistant cells. A role for Bcl-X(L). J Biol Chem 2004;279:9215–21.
[33] Dehdashti F, Mintun MA, Lewis JS, et al. In vivo assessment of tumor hypoxia in lung cancer with 60Cu-ATSM. Eur J Nucl Med Mol Imaging 2003;30:844–50.
[34] Dehdashti F, Grigsby PW, Mintun MA, Lewis JS, Siegel BA, Welch MJ. Assessing tumor hypoxia in cervical cancer by positron emission tomography with 60Cu-ATSM: relationship to therapeutic response — a preliminary report. Int J Radiat Oncol Biol Phys 2003;55:1233–8.
[35] Chao KS, Bosch WR, Mutic S, et al. A novel approach to overcome hypoxic tumor resistance: Cu-ATSM-guided intensity-modulated radiation therapy. Int J Radiat Oncol Biol Phys 2001;49:1171–82.
[36] Lewis J, Laforest R, Buettner T, et al. Copper-64-diacetyl-bis(N4-methylthiosemicarbazone): an agent for radiotherapy. Proc Natl Acad Sci U S A 2001;98:1206–11.
[37] Aft RL, Lewis JS, Zhang F, Kim J, Welch MJ. Enhancing targeted radiotherapy by copper(II)diacetyl-bis(N4-methylthiosemicarbazone) using 2-deoxy-D-glucose. Cancer Res 2003;63:5496–504.
[38] Obata A, Kasamatsu S, Lewis JS, et al. Basic characterization of 64Cu-ATSM as a radiotherapy agent. Nucl Med Biol 2005; 32:21–8.

資料(6)